

Post-weaning high-fat diet accelerates kidney injury, but not hypertension programmed by maternal diabetes

Yessoufou Aliou¹, Min-Chun Liao¹, Xin-Ping Zhao¹, Shiao-Ying Chang¹, Isabelle Chenier¹, Julie R. Ingelfinger² and Shao-Ling Zhang¹

BACKGROUND: The aim of this study was to establish the underlying mechanisms by which a post-weaning high-fat diet (HFD) accelerates the perinatal programming of kidney injury occurring in the offspring of diabetic mothers.

METHODS: Male mice, offspring of nondiabetic and diabetic dams were fed with normal diet (ND) or HFD from 4 to 20 wk of age. Rat renal proximal tubular cells were used *in vitro*.

RESULTS: On ND, the offspring of dams with severe maternal diabetes had an intrauterine growth restriction (IUGR) phenotype and developed mild hypertension and evidence of kidney injury in adulthood. Exposing the IUGR offspring to HFD resulted in rapid weight gain, catch-up growth, and later to profound kidney injury with activation of renal TGF β 1 and collagen type IV expression, increased oxidative stress, and enhanced renal lipid deposition, but not systemic hypertension. Given our data, we speculate that HFD or free fatty acids may accelerate the process of perinatal programming of kidney injury, via increased CD36 and fatty acid-binding protein 4 expression, which may target reactive oxygen species, nuclear factor-kappa B, and TGF β 1 signaling *in vivo* and *in vitro*.

CONCLUSION: Early postnatal exposure to overnutrition with a HFD increases the risk of development of kidney injury, but not hypertension, in IUGR offspring of dams with maternal diabetes.

Diabetes during pregnancy, whether gestational or pregestational diabetes (type 1 or type 2), results in offspring at high risk of developing hypertension, cardiovascular disease, and chronic kidney disease in adult life. This phenomenon, termed perinatal programming, in which intrauterine events are associated with later adverse changes, has attracted much attention (1–3). Substantial epidemiologic data have also suggested that the offspring whose mothers were diabetic during pregnancy are susceptible to metabolic disturbances induced by postnatal overnutrition, as seen with high-fat diet (HFD) or with increased caloric intake in early life (1–4).

Women who have diabetes during pregnancy and/or are obese and hyperinsulinemic are at risk of delivering

macrosomic newborns (high birth weight), and both short- and long-term outcomes of macrosomic neonates are influenced by postnatal overnutrition (1–4). In high-birth-weight neonates, subsequent growth in infancy and risk of becoming obese or diabetic are directly and linearly linked—e.g., the higher the birth weight, the greater the risk of overweight and metabolic disturbances later in life (1–4). In contrast, pregnant women with severe, uncontrolled diabetes or diabetic complications, such as diabetic nephropathy and/or retinopathy, are at high risk of having a macrosomic fetus (i.e., a fetus with intrauterine growth restriction (IUGR)) (5,6). Such infants may be markedly small for dates; but many develop excessive weight gain and increased fat deposition in early infancy, a proxy for neonatal overnutrition (7,8). However, the long-term outcome of IUGR offspring who experience overnutrition in early life is incompletely delineated.

Previously, we demonstrated in a mouse model that severe maternal diabetes (defined as maternal blood glucose concentration \sim 30 mmol/l) is linked to IUGR in offspring (mean decrease 20% of birth weight). Such offspring showed impaired nephrogenesis resulting in nascent nephron deficiency in neonate and manifested hypertension, glucose intolerance, and kidney injury in adulthood. The possible mechanisms involved in those phenomena include reactive oxygen species (ROS) elevation and activation of the nuclear factor-kappa B (NF- κ B), TGF β 1, and p53 pathways (9–13).

Compelling evidence from both experimental (14–16) and human studies (17,18) have suggested that perirenal and/or visceral fat depots may mediate the development of chronic kidney disease and hypertension. CD36 (19–22) and fatty acid-binding protein 4 (Fabp4) (23–27) may mediate chronic inflammation, insulin resistance, oxidant stress, and fibrosis involved in proatherogenic hyperlipidemic states such as obesity. In this study, we followed these affected IUGR offspring from 4 to 20 wk of age and compared the metabolic impacts of post-weaning diet (HFD vs. normal diet (ND)) on handling of lipoproteins, hypertension, and renal function. Focusing on the kidney, we hypothesized that feeding the affected IUGR offspring with HFD after weaning would exacerbate

The first two authors contributed equally to this work.

¹Centre de recherche du Centre hospitalier de l'Université de Montréal (CRCHUM), Université de Montréal, Montréal, Quebec, Canada; ²Pediatric Nephrology Unit, Massachusetts General Hospital and Harvard Medical School Boston, Boston, Massachusetts. Correspondence: Shao-Ling Zhang (shao.ling.zhang@umontreal.ca)

Received 10 January 2015; accepted 24 August 2015; advance online publication 9 December 2015. doi:10.1038/pr.2015.236

the metabolic perturbations and kidney injury in adulthood; we also hypothesized that alteration of renal CD36 and Fabp4 gene expression is associated with these adverse effects.

RESULTS

Growth Curves of Offspring

We compared the growth pattern of four subgroups of male offspring of nondiabetic (control) and diabetic dams—e.g., control offspring on ND (Con-ND, $N = 17$); control offspring on HFD (Con-HF, $N = 15$); diabetic offspring on ND (Dia-ND, $N = 12$), and diabetic offspring on HFD (Dia-HF, $N = 12$). Similar to previous reports (9–11), Dia-ND mice born with IUGR continued to have lower body weight (BW, g) throughout life (mean BW in cross-section time-point measurement decreased 20%; $P \leq 0.01$; **Figure 1a**). HFD increased BW of both Con-HF and Dia-HF animals over time. Offspring of diabetic dams were more sensitive to HFD as compared to those of control dams, as they showed the steepest climb in BW—i.e., a catch-up pattern from 4 to 5 wk ($P < 0.05$; **Figure 1c**). In contrast, significant BW gain in

Con-HF mice (vs. Con-ND mice) began only at 8 wk of age ($P < 0.05$; **Figure 1b**).

Metabolic Parameters

At 20 wk, as compared with Con-ND mice, Dia-ND animals had increased plasma levels of nonesterified fatty acids (NEFA) (**Figure 1d**; $P < 0.01$), triglycerides (**Figure 1e**; $P < 0.01$), and cholesterol (**Figure 1f**; $P < 0.05$), but not insulin (**Figure 1g**). HFD was associated with elevated plasma levels of NEFA ($P < 0.05$), triglycerides ($P < 0.05$), cholesterol ($P < 0.01$), and insulin ($P < 0.01$) in Con-HF animals, but this was not seen in Dia-HF groups (**Figure 1d–g**). Intraperitoneal glucose tolerance test (**Figure 1h,i**) and insulin sensitivity test (IST) (**Figure 1j**) were performed at 19 wk before animals were killed. The fasting blood glucose concentration (mmol/l) at baseline of the four subgroups did not differ from each other (Con-ND (8.31 ± 0.34) vs. Dia-ND (8.0 ± 0.36); Con-HF (10.45 ± 0.47) vs. Dia-HF (9.71 ± 0.53); **Figure 1h**). HFD impaired glucose tolerance in both Con-HF and Dia-HF offspring at similar levels (**Figure 1h,i**; $P < 0.01$), despite the fact that Dia-ND already

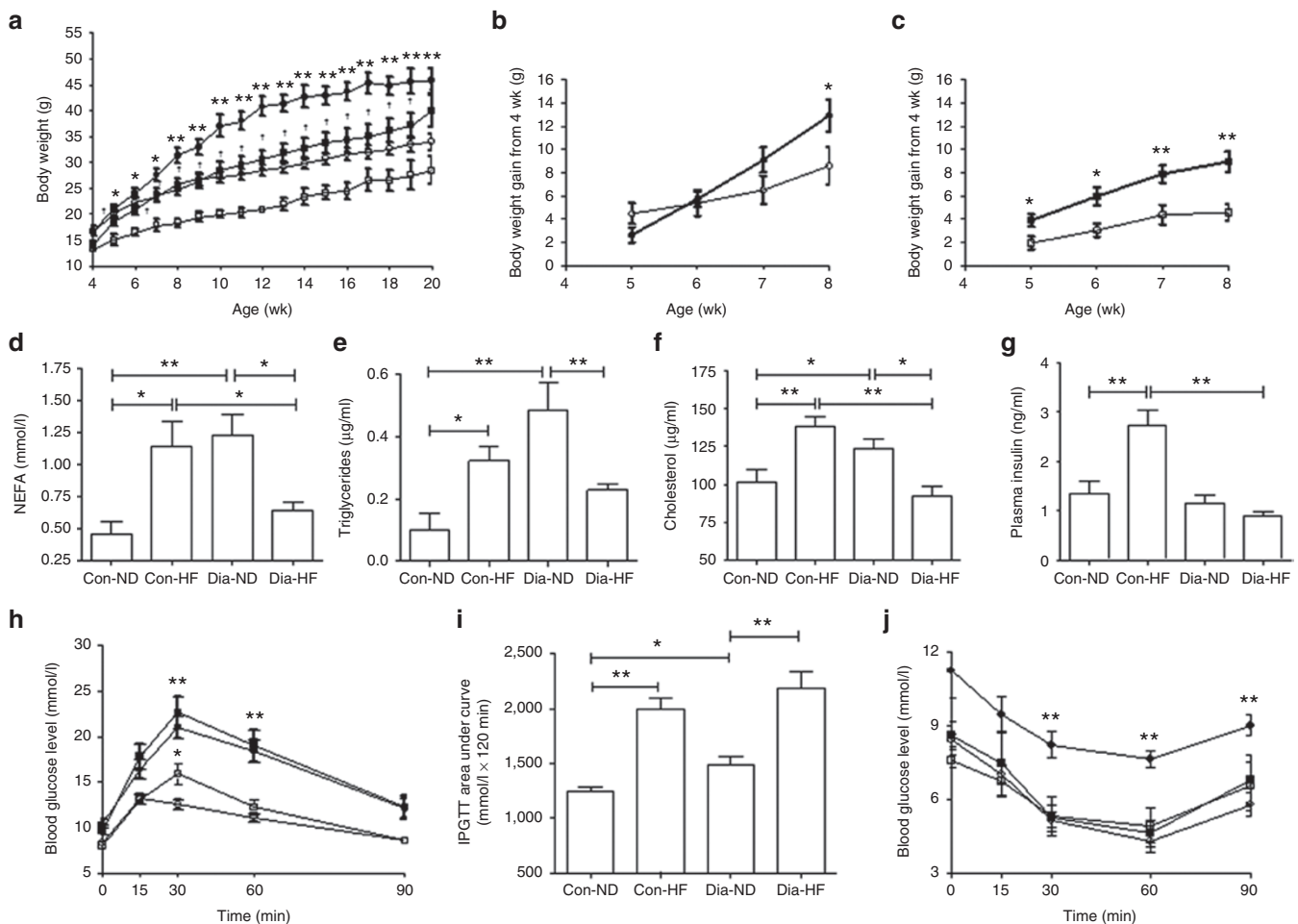


Figure 1. Metabolic parameters in offspring. (a) Growth follow-up in four subgroups of male offspring from the age of 4 to 20 wk. (○) Con-ND; (●) Con-HF; (□) Dia-ND; (■) Dia-HF; *, $P \leq 0.05$; ** $P \leq 0.01$ vs. Con-ND; * $P \leq 0.01$ vs. Dia-ND. (b,c) Body weight gain in male offspring from the age of 4 to 8 wk (b: offspring from control dams and c: offspring from diabetic dams). (○) Con-ND; (●) Con-HF; (□) Dia-ND; (■) Dia-HF; * $P \leq 0.05$; ** $P \leq 0.01$. (d–g) Plasma metabolic profile measurements (d: NEFA (mmol/l); e: triglycerides (µg/ml); f: cholesterol (µg/ml); and g: insulin (ng/ml)) in four subgroups of 20-wk-old male offspring. * $P \leq 0.05$; ** $P \leq 0.01$. (h) IPGTT measurement. (○) Con-ND; (●) Con-HF; (□) Dia-ND; (■) Dia-HF; * $P \leq 0.05$; ** $P \leq 0.01$ vs. Con-ND. (i) IPGTT area under curve; * $P \leq 0.05$; ** $P \leq 0.01$. (j) IST measurement. (○) Con-ND; (●) Con-HF; (□) Dia-ND; (■) Dia-HF; ** $P \leq 0.01$; * $P \leq 0.01$ vs. Con-ND. Values represent the mean \pm SEM. IPGTT, intraperitoneal glucose tolerance test.

displayed a mild degree of impaired glucose tolerance ($P < 0.05$) when compared with Con-ND, as we also showed previously (10). Con-HF animals showed less insulin sensitivity through the entire IST procedure ($P < 0.01$), while a similar IST pattern was observed for the other three groups (Figure 1j).

Mean Systolic Blood Pressure

Longitudinal measurement of systolic blood pressure (SBP) (Figure 2a), recorded from 6 to 20 wk of age, revealed that Dia-ND have significantly higher SBP over the follow-up period when compared with Con-ND, as previously reported (10). HFD animals displayed normal SBP (mm Hg) at 10 to 20 wk of age, irrespective of whether they were offspring of dams with maternal diabetes or not (Figure 2a).

Kidney Function and Adipocyte Morphology

As compared with Con-ND mice, Dia-ND animals exhibited significantly increased ($P \leq 0.05$) urinary albumin/creatinine ratio (Figure 2b) and glomerular filtration rate (GFR; $P \leq 0.01$; Figure 2c).

HFD was associated with a significantly increased albumin/creatinine ratio ($P \leq 0.05$) in both groups of offspring

compared with respective ND groups (Figure 2b). However, HFD was not associated with changes of GFR/ tibia length (TL) ratio in either control or diabetic animals (Figure 2c). The kidney weight/TL (mm) ratio among the four groups of animals remains unchanged either in ND or HFD condition.

As compared with Con-ND, Dia-ND mice had a decreased number of adipocytes ($P < 0.01$) collected from both perirenal and visceral fat. These changes were more pronounced in HFD offspring (Con-HF; $P < 0.01$; Dia-HF; $P < 0.05$; Figure 2d,e).

Renal Expression of Extracellular Matrix Protein

Consistent with previous reports (9,10), Dia-ND offspring at 20 wk showed enhanced extracellular matrix protein accumulation seen by periodic acid–Schiff (Figure 3a) and Masson’s trichrome (Figure 3b) staining, resulting in glomerulosclerosis ($P < 0.01$; Figure 3h) and tubulointerstitial injury ($P < 0.05$; Figure 3i).

Our immunohistochemistry (IHC) data indicate that the kidneys of Dia-ND offspring also had increased expression of TGFβ1 (Figure 3c) and collagen type IV (Figure 3d) localized to both glomeruli ($P < 0.01$; Figure 3j) and tubulointerstitium ($P < 0.05$; Figure 3k). And most importantly, HFD enhanced

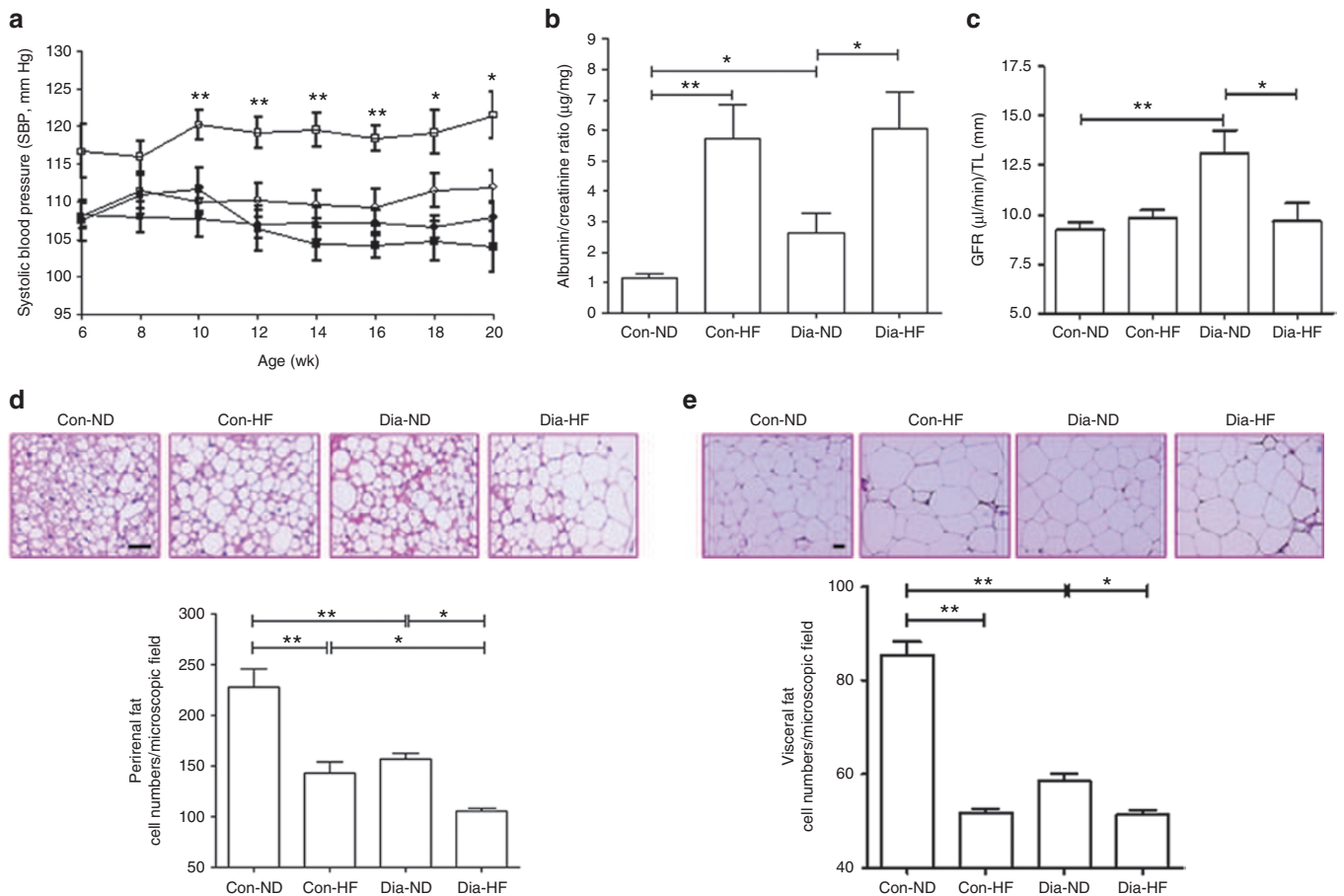


Figure 2. Blood pressure, renal function, and adipocyte morphology. (a) Longitudinal SBP measurement. (c) Con-ND; (●) Con-HF; (□) Dia-ND; (■) Dia-HF; * $P \leq 0.05$; ** $P \leq 0.01$ vs. Con-ND. (b) Urinary ACR measurement; * $P \leq 0.05$; ** $P \leq 0.01$. (c) GFR/TL ratio; * $P \leq 0.05$; ** $P \leq 0.01$. (d) H&E staining- perirenal fat (magnification: $\times 200$) with semi-quantitation of adipocyte number per microscopic field ($N = 10$ fields per animal). * $P \leq 0.05$; ** $P \leq 0.01$. (e) H&E staining- visceral fat (magnification: $\times 100$) with semi-quantitation of adipocyte number per microscopic field ($N = 10$ fields per animal). * $P \leq 0.05$; ** $P \leq 0.01$. Values represent the mean \pm SEM. ACR, albumin/creatinine ratio; GFR, glomerular filtration rate; H&E, hematoxylin and eosin; SBP, systolic blood pressure; TL, tibia length.

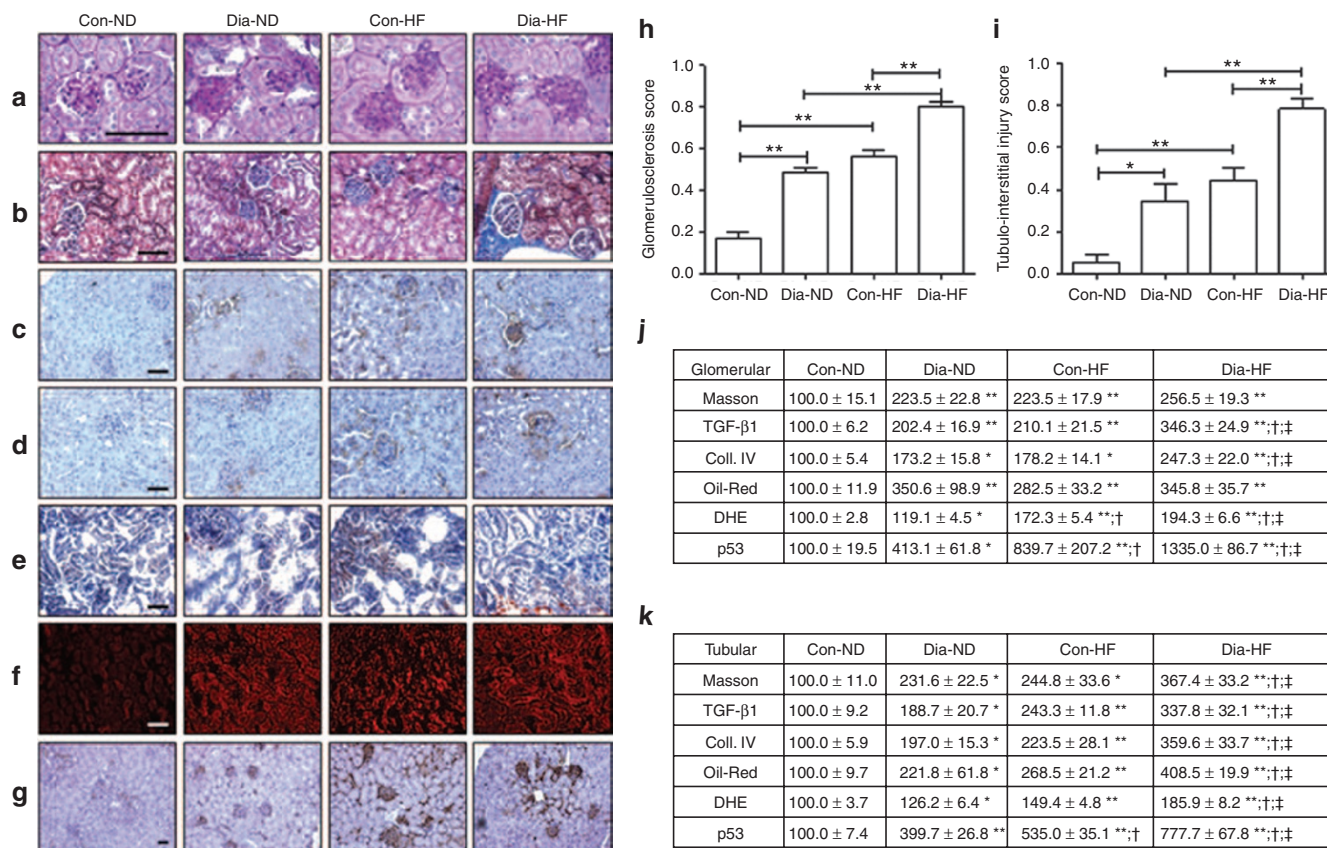


Figure 3. Renal morphology. (a) PAS staining (magnification: $\times 600$). (b) Masson's trichrome staining (magnification: $\times 200$). (c) IHC-TGF β 1 staining (magnification: $\times 200$). (d) IHC-collagen type IV (magnification: $\times 200$). (e) Oil red deposition (magnification: $\times 200$). (f) DHE staining (magnification: $\times 200$). (g) IHC-p53 staining (magnification: $\times 100$). (h) Classic scoring of glomerulosclerosis based on PAS images. Grade 0, normal glomeruli; grade 1, presence of mesangial expansion/thickening of the basement membrane. (i) Classic scoring of tubulointerstitial injury based on PAS images. Grade 0, normal tubules; grade 1, the tubulointerstitial lesions involving less than 25% of the field. (j-k) Semi-quantitation of the relative staining values in both (j) glomerular and (k) tubular compartment. The value in Con-ND animals was 100% \pm SEM. * $P \leq 0.05$; ** $P \leq 0.01$ vs. Con-ND; † $P \leq 0.05$ vs. Dia-ND; ‡ $P \leq 0.05$ vs. Con-HF. Values represent the mean \pm SEM. DHE, dihydroethidium; PAS, periodic acid-Schiff.

these changes in both groups of offspring ($P < 0.01$), particularly in the kidneys of Dia-HF mice.

Oil Red Staining, Oxidative Stress, and Apoptosis in Kidney

Within the kidneys of HFD animals (Con-HF vs. Dia-HF) at 20 wk of age, there was increased oil red staining (Figure 3e), elevated oxidative stress on dihydroethidium staining (e.g., the non-fluorescent dihydroethidium is oxidized to fluorescent ethidium by superoxide anion ($O_2^{\cdot -}$)) (Figure 3f) and augmented apoptotic events on p53-IHC staining (Figure 3g) in both glomeruli ($P < 0.05$; Figure 3j) and tubulointerstitium ($P < 0.05$; Figure 3k).

Renal CD36 and Fabp4 Expression

As compared with Con-ND mice, renal CD36 (Figure 4a, mRNA; Figure 4c, protein) and Fabp4 (Figure 4b, mRNA; Figure 4d, protein) expression were increased in renal cortex in Dia-ND ($P < 0.05$) and both HFD-fed groups (Con-HF vs. Dia-HF). Moreover, IHC staining (Figure 5) revealed that increased CD36 and Fabp4 were predominantly localized in the proximal tubular cells, particularly in the kidneys of Dia-HF mice (Figure 5a) colocalizing with aquaporin 1 immunostaining (Figure 5b,c).

In Vitro Studies

We performed *in vitro* experiments using bovine serum albumin (BSA)-bound sodium palmitate (BSA-PA) to treat immortalized rat renal proximal tubular cells (IRPTCs) (9) to confirm our *in vivo* observations. BSA-PA stimulated both CD36 and Fabp4 protein expression in a dose-dependent manner (Figure 6a) in IRPTCs. Moreover, BSA-PA (125 μ mol/l) was associated with significantly induced ROS generation (Figure 6b; $P < 0.01$), increased apoptosis (Caspase 3 activity, Figure 6c, $P < 0.01$; Hoechst staining, Figure 6d, $P < 0.01$; and phosphorylation of p53, Figure 6e) and augmented NF- κ B (i.e., p50/p65) as well as TGF β 1 protein expression (Figure 6e, $P < 0.01$) in IRPTCs.

DISCUSSION

This study indicates that IUGR offspring of diabetic dams post-weaning fed with HFD showed "rapid" weight gain, catch-up growth, and subsequently displayed features of profound kidney injury associated with increased CD36 and Fabp4 expression. However, they did not have hypertension in adulthood.

In agreement with most human and experimental observations (1–3,7,8), we observed "rapid" catch-up growth in young

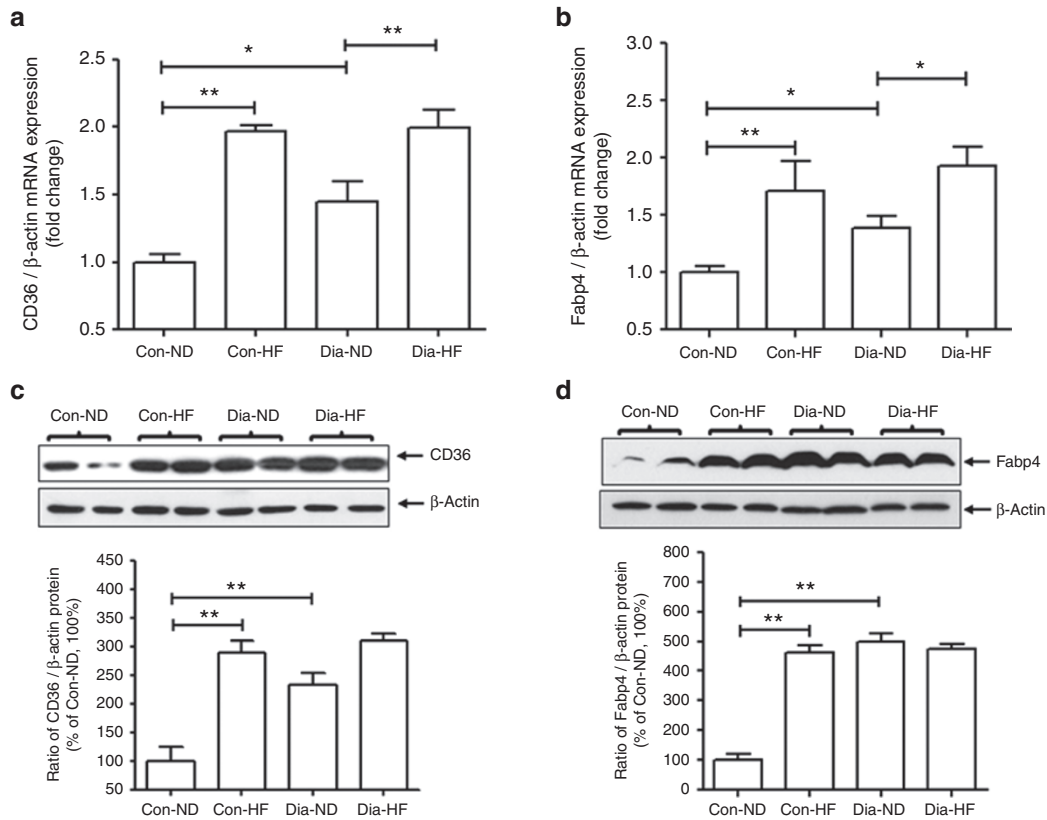


Figure 4. Renal CD36 & Fabp 4 gene expression. (a–c) Renal CD36 and (b–d) Fabp4 gene expression in the renal cortex of four subgroups of 20-wk-old male offspring. (a and b) qRT-PCR analysis. (c and d) Western blot analysis. The relative densities of CD36 and Fabp4 were compared with their own β -actin mRNA or protein. The values of Con-ND animals were considered as 100%. Each point represents the mean \pm SEM of three independent experiments. * $P \leq 0.05$; ** $P \leq 0.01$.

Dia-HF offspring from 5 to 8 wk of age. Con-HF offspring became obese over time, with elevated plasma lipids at 20 wk of age (i.e., NEFA, triglycerides, and cholesterol), whereas Dia-HF offspring had similar BW and lipid levels as Con-ND at 20 wk of age, underscoring the finding that postnatal HFD feeding has a differential impact on the growth pattern in the offspring of both nondiabetic and diabetic dams.

Similar observations were also reported in the small litter rat model in which smaller young offspring were exposed to HFD feeding (4,28,29). The implications of those findings were that HFD enhanced insulin sensitivity and fatty-acid oxidation in the skeletal muscle and increased plasma levels of leptin, insulin, and adiponectin to maintain BW and metabolic homeostasis in the normal range (4,28,29). Since increasing lipid oxidation might improve insulin sensitivity (30,31), in this study, when compared with Con-HF mice, Dia-HF animals with normal lipid metabolism and plasma insulin levels had a rapid insulin response and higher insulin sensitivity by IST measurement, hinting that enhanced lipid oxidation might have occurred in these animals. Taken together, our data suggest that Dia-HF animals might use HF as the fuel or energy to balance their BW and metabolism.

In humans, increased intrarenal and perirenal fat is associated with an increased risk of hypertension and chronic kidney disease (17,18). However, the observations of obesity-induced hypertension in animals are varied (32). For instance, Kennedy

et al. (32) recently reviewed blood pressure responses in obese mouse models such as *Lep^{ob/ob}*, *LepR^{db/db}*, and HFD-induced obesity; responses of blood pressure include an increase, decrease, or no change, largely depending on strain, sex, age, environment, and the method of measuring BP. In this study, we did not observe an impact from HFD on the development of hypertension in either Con-HF or Dia-HF mice; our results are similar to reported observations in 5 out of 6 nephrectomized rats fed with HFD (33) and obese ZSF1 rats (34). Previously, the mild hypertension we noted in Dia-ND animals (9,10) was mainly because of renal hypertrophy related to renal hyperfiltration with increased GFR. However, we noted that Dia-HF mice at 20 wk of age showed kidney weight/TL and GFR/TL ratios comparable to Con-ND animals, which might be a partial explanation for their normotensive status.

Renal injury has been reported previously in our Dia-ND mice (9–13). In this work, we found that HFD augmented TGF β 1 and collagen IV gene expression, increased renal lipid accumulation, as well as heightened oxidative stress in both glomerular and tubular compartments in the kidneys of Dia-HF mice, resulting in significant glomerulosclerosis, tubular fibrosis, and apoptosis. Although our findings are consonant with other reports (14–16), results reported in remnant kidney rats receiving HFD (33) seem to ameliorate these parameters/pathways to prevent kidney injury. Currently, we do not have further explanation for this discrepancy beside species differences.

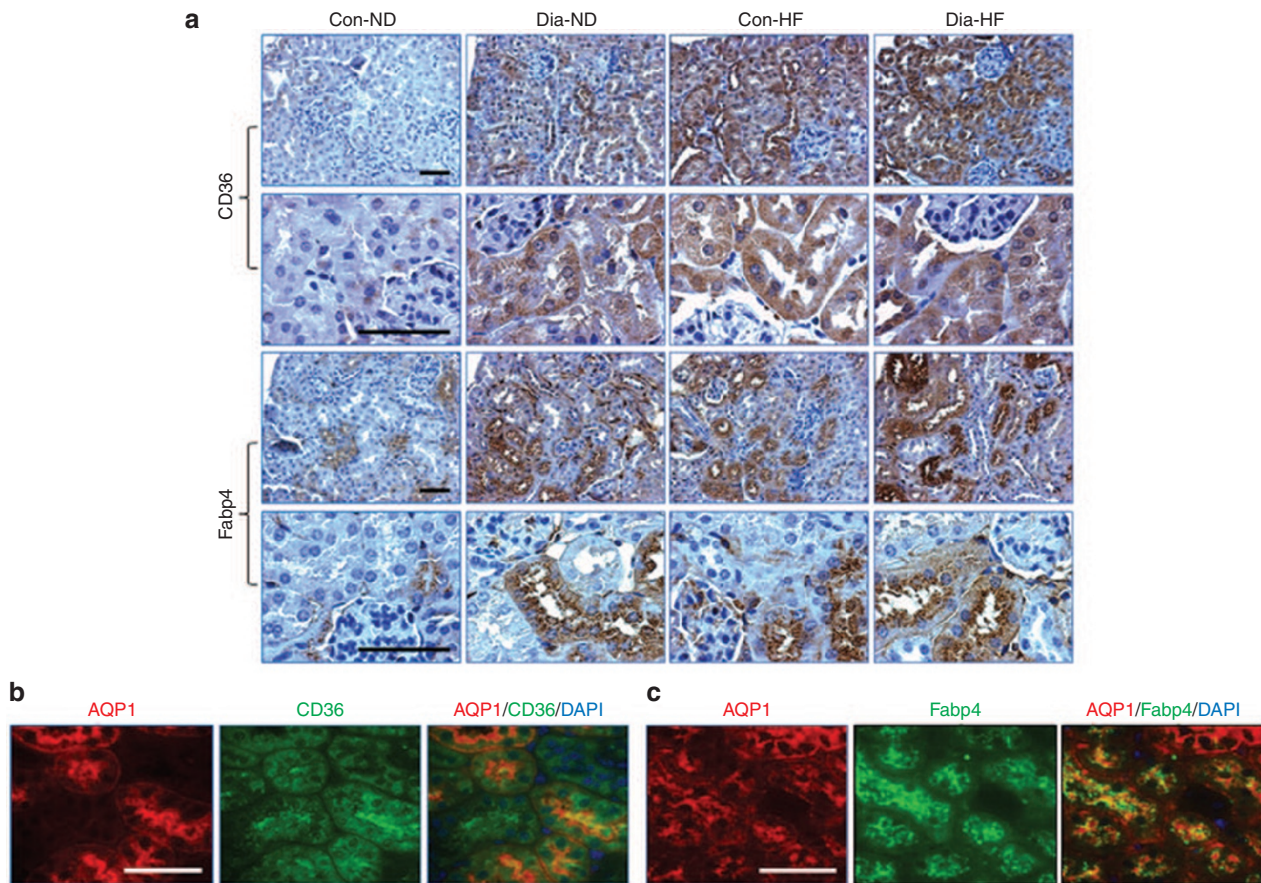


Figure 5. Renal CD36 & Fabp 4 localization. (a) IHC staining images of CD36 and Fabp4 in the kidneys of four subgroups of 20 wk-old male offspring (magnification: $\times 200$; $\times 600$). (b) The colocalization of AQP1 (red) with CD36 (green) in the kidneys of Dia-HF animals (magnification: $\times 600$). (c) The colocalization of AQP1 (red) with Fabp4 (green) in the kidneys of Dia-HF animals (magnification: $\times 600$). AQP1, aquaporin 1; Fabp4, fatty acid-binding protein 4.

Emerging evidence suggested that CD36 (19–22) and Fabp4 (23–27) are highly implicated in the pathogenesis of HFD-induced cell damage. For example, intrarenal CD36 has been identified as a novel mediator in renal diseases associated with proteinuria and renal dysfunction (35). The elevated level of serum/plasma/urinary Fabp4 is considered a predictor or biomarker for renal dysfunction in diabetes and cardiovascular diseases (23–27). Hence, we further hypothesized that these affected IUGR offspring fed with HFD would develop metabolic perturbations and kidney injury in adulthood that might be associated with alterations of both renal CD36 and Fabp4 gene expression.

Our data showed that HFD enhanced renal CD36 and Fabp 4 expression, which predominantly localized to PTCs (confirmed by colocalization in PTCs with the PTC biomarker, aquaporin 1), but not in glomeruli, suggesting that it is plausible that apparent CD36- and Fabp4-mediated PTC changes might be secondary to proteinuria and/or lipiduria.

We validated our *in vivo* findings with *in vitro* studies in IRPTCs and investigated the functional impact of free fatty acids (i.e., BSA-PA) on renal CD36 and Fabp 4 expression and its related molecular mechanism(s). We observed that BSA-PA stimulated both CD36 and Fabp4 protein expression in a dose-dependent manner in IRPTCs. CD36 has been shown to

mediate PTC apoptosis (36) and to influence the binding and uptake of albumin in PTCs to promote proteinuria (35). The activated CD36 in PTCs targets JNK, ROS, and inflammatory cytokines to facilitate renal dysfunction (22). CD36 deficiency attenuates TGF β 1 signaling, NF- κ B activity, and renal fibrosis in hypercholesterolemic mice (37), whereas CD36 overexpression leads to lipid accumulation in PTCs (20). On the other hand, Fabp4 was reported to be actively expressed in the peritubular and glomerular region to mediate renal dysfunction in diseased kidney (26,27). Fabp4, via the ER stress-JNK pathway, mediated vascular inflammation in the pathogenesis of cardiovascular disorders associated with obesity and diabetes (38). Thus, we tested those potential mechanisms in IRPTCs in culture, and our data suggested that BSA-PA induced ROS generation, enhanced apoptosis (via phosphorylation of p53), and activated NF- κ B (i.e., p50/p65) and TGF β 1 protein expression in IRPTCs. These data would support the concept that CD36 and Fabp 4, induced by free fatty acids, may contribute to the substantial PTC damages resulting in tubulointerstitial fibrosis and apoptosis.

Taken together, our observations suggest a synergistic contribution by CD36 and Fabp4 to renal dysfunction and injury. Our data indicate that, in addition to HFD-induced glomerular injury, HFD via increased CD36 and Fabp4 expression

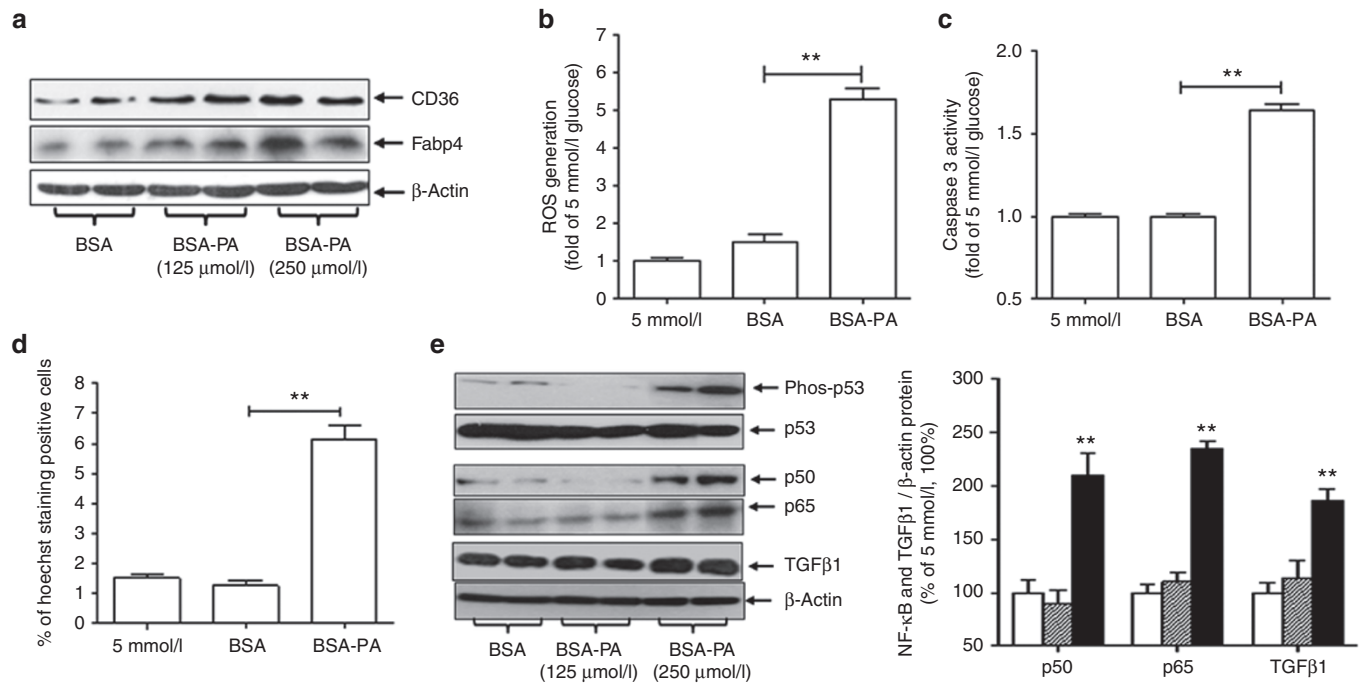


Figure 6. BSA-PA effects in IRPTCs. (a) CD36 and Fabp4 protein expression analyzed by western blot. (b) ROS generation. (c) Caspase 3 activity assay. (d) Quantification of Hoechst staining-positive cells. (e) Western blot of phosphorylation of p53, NF-κB (i.e., p50/p65), and TGFβ1 protein expression. The relative densities of gene expression were compared with their own β-actin, and the gene expression protein ratio in 5 mmol/l glucose medium was considered as 100%. IRPTC in 5 mmol/l glucose (white bar); BSA (shadowed bar), and BSA-PA (black bar). Each point represents the mean ± SEM of three independent experiments. **P* ≤ 0.05; ***P* ≤ 0.01. BSA-PA, bovine serum albumin-bound sodium palmitate; IRPTC, immortalized rat renal proximal tubular cell; NF-κB, nuclear factor-kappa B.

in PTCs may target ROS, NF-κB, and TGFβ1 signaling to accelerate the process of maternal diabetes-induced perinatal programming of kidney injury. In conclusion, early postnatal exposure to HFD in IUGR offspring of diabetic dams increases the risk of development of subsequent kidney injury, but not hypertension.

METHODS

Animal Models

In our established *in vivo* murine model of maternal diabetes induced by a single i.p. streptozotocin (150 mg/kg) injection on gestational day E13 (9–13), male offspring of diabetic dams displayed more pronounced programming phenotypes; hence, we chose to focus on males for this designed HFD study. Male offspring from nondiabetic and diabetic C57/BL6 mice were fed with normal chow (ND) (18% protein with 6.2% fat, calories from protein 24%, fat 18%, and carbohydrate 58%; Harlan Teklad, Montreal, Canada) or HFD (20.5% protein with 36% fat, calories from protein 14%, fat 60%, and carbohydrate 26%; Bio-Serv, Flemington, NJ) from 4 wk until 20 wk of age. All animals were killed at 20 wk of age with high CO₂, and the kidneys removed immediately. BW (g), kidney weight (mg), and TL (mm) were rapidly recorded. The biological samples were processed, collected, and stored accordingly for analysis. Kidneys were either quickly frozen in OCT or fixed overnight in 4% paraformaldehyde at 4 °C before paraffin embedding.

Animal care and the procedures utilized were approved by the Institutional Animal Care Committee of the CRCHUM. Mice were housed under standard humidity and lighting conditions (12-h light-dark cycles) with free access to water and food designed.

Biochemical and Physiological Studies

Plasma NEFA level (mmol/l) was measured using an NEFA kit that detects a variety of free fatty acids (Wako Chemical, Osaka, Japan). Plasma triglycerides (mg/ml) were determined by GPO Trinder

kit (Sigma Aldrich, St Louis, MO). Plasma cholesterol (μg/ml) was assessed by the amplex red cholesterol assay kit (Invitrogen, Burlington, Canada). Plasma insulin was measured by mouse ultra-sensitive insulin ELISA jumbo kit (Alpco Diagnostics, Salem, NH).

Blood glucose levels were measured with an Accu-Chek Performa glucose meter (Roche Diagnostics, Laval, Canada) in the morning after a 4-h fast, as previously reported (9,10). Mean SBP was monitored by the tail-cuff method with the Visitech BP-2000 Blood Pressure Analysis System for mice (Visitech System, Apex, NC) in longitudinal fashion to minimize stress-related hypertension (9,10). The animals were acclimated to SBP measurement with a 2 wk period of pretraining starting at 4 wk of age (SBP measured 15 times/animal/day, thrice weekly), followed by actual measurement of SBP thrice weekly from 6 wk until 20 wk of age.

Intraperitoneal Glucose Tolerance Test and IST

Intraperitoneal glucose tolerance test and IST were performed according to a standard protocol. Blood glucose was quantified with an Accu-Chek Performa glucose meter. Briefly, intraperitoneal glucose tolerance test was performed after a 6-h fast; 1 mg/g body glucose was injected intraperitoneally, and blood glucose levels were measured at 0, 15, 30, 60, and 120 min. IST was initiated after a 4-h fast. Humulin R (Eli Lilly Canada, Toronto, Canada; 0.75 units/kg) was injected intraperitoneally, and blood glucose levels were measured at 0, 15, 30, 60, and 90 min.

Glomerular Filtration Rate

As reported previously (9), we measured GFR in 20 wk-old male animals by the fluorescein isothiocyanate-inulin method, recommended by the Diabetic Complications Consortium. Urine samples, collected from mice individually housed in metabolic cages, were assayed for albumin/creatinine ratio (ELISA, Albuwell and Creatinine Companion, Exocell, Philadelphia, PA), as reported previously (9,10).

Histology

We assessed hematoxylin and eosin staining of adipocyte collected from both visceral and perirenal fat. The number of adipocytes

displayed in microscopic fields ($N = 10$ fields per animal) were quantitated in a randomized and blinded fashion. Renal morphology was assessed with periodic acid–Schiff and Masson's trichrome staining (9,10). IHC was performed by the standard avidin–biotin–peroxidase complex method (Santa Cruz Biotechnologies, Santa Cruz, CA), as described elsewhere (9,10). The antibodies used included polyclonal p53 and aquaporin 1 (Santa Cruz Biotechnologies); anti-TGF β 1 antibody (R&D Systems, Burlington, Canada); monoclonal anticollagen type IV antibody (Chemicon International, Temecula, CA); polyclonal CD36 antibody (Abcam, Cambridge, MA); Fabp4 antibody (R&D Systems). Oxidative stress *in vivo* was assessed by dihydroethidium (Sigma-Aldrich, Oakville, Canada) staining in frozen kidney sections as reported previously (13). The classic scoring of glomerulosclerosis (scale from 0 to 4) (39) and tubulo-interstitial injury (scale from 0 to 3) (40) was based on periodic acid–Schiff images. The semi-quantitation of the relative staining values was performed by NIH Image J software (Bethesda, MD) (9,10). The images ($N = 6$ –8 per animal) were analyzed and quantitated in a randomized and blinded fashion.

Real-Time Quantitative PCR

Total RNA extracted from freshly isolated renal cortex was assayed for gene expression by real-time quantitative PCR and calculated using the $\Delta\Delta C_t$ method, as reported previously (9–13). The Fast SYBR green mastermix kit and the 7500 Fast real-time PCR system (Applied Biosystems, Life Technologies, Foster City, CA) were employed for this purpose (9–13). The primer sequences are listed as: CD36 (S), 5'-catattggtcaagccagctag-3'; CD36 (AS), 5'-agcaacaa-catcaccactcc-3'; Fabp4 (S), 5'-aaggtgaagagcatcataaccct-3'; Fabp4 (AS), 5'-tcacgcttataacacatcc-3'.

In Vitro Studies

The IRPTC line (passages 15–18) reported previously (9) was employed for our *in vitro* studies. Caspase-3 activity, ROS generation, and Hoechst staining were measured in IRPTCs treated with or without BSA (fatty acid free; Sigma-Aldrich) or BSA-PA (Sigma-Aldrich) overnight. The preparation of BSA-PA (125 $\mu\text{mol/l}$ and 250 $\mu\text{mol/l}$) was described in detail by Roduit *et al* (41). The antibodies used for western blot included NF- κ B (p50/p65), p53, and TGF β 1 from Santa Cruz Biotechnology; anti-phospho-p53 (Ser 15) from Abcam.

Statistical Analysis

Statistical significance between the experimental groups was analyzed by one-way ANOVA, by using Graphpad Software, Prism 5.0 (La Jolla, CA). A probability level of $P \leq 0.05$ was considered to be statistically significant and followed by a Bonferroni analysis with adjustment for multiple comparisons (9–13).

ACKNOWLEDGMENTS

The authors owe special thanks to John S.D. Chan (CRCHUM, Montreal, QC, Canada) for his unconditional support and valuable comments on this manuscript. Editorial assistance was provided by the CRCHUM's Research Support Office.

STATEMENT OF FINANCIAL SUPPORT

This project was supported by grants to S.-L.Z. from the Canadian Institutes of Health Research (MOP115025) and Canadian Diabetes Association (OG-3-13-4073-SZ).

Disclosure: None.

REFERENCES

1. Plagemann A. Maternal diabetes and perinatal programming. *Early Hum Dev* 2011;87:743–7.
2. Plagemann A, Harder T, Rodekamp E, Kohlhoff R. Rapid neonatal weight gain increases risk of childhood overweight in offspring of diabetic mothers. *J Perinat Med* 2012;40:557–63.
3. Plagemann A, Harder T, Schellong K, Schulz S, Stupin JH. Early postnatal life as a critical time window for determination of long-term metabolic health. *Best Pract Res Clin Endocrinol Metab* 2012;26:641–53.
4. Spencer SJ. Early life programming of obesity: the impact of the perinatal environment on the development of obesity and metabolic dysfunction in the offspring. *Curr Diabetes Rev* 2012;8:55–68.
5. Holemans K, Aerts L, Van Assche FA. Fetal growth restriction and consequences for the offspring in animal models. *J Soc Gynecol Investig* 2003;10:392–9.
6. Van Assche FA, Holemans K, Aerts L. Long-term consequences for offspring of diabetes during pregnancy. *Br Med Bull* 2001;60:173–82.
7. Perälä MM, Männistö S, Kaartinen NE, *et al*. Body size at birth is associated with food and nutrient intake in adulthood. *PLoS One* 2012;7:e46139.
8. Crowther NJ, Cameron N, Trusler J, Toman M, Norris SA, Gray IP. Influence of catch-up growth on glucose tolerance and beta-cell function in 7-year-old children: results from the birth to twenty study. *Pediatrics* 2008;121:e1715–22.
9. Chang SY, Chen YW, Zhao XP, *et al*. Catalase prevents maternal diabetes-induced perinatal programming via the Nrf2–HO-1 defense system. *Diabetes* 2012;61:2565–74.
10. Chen YW, Chenier I, Tran S, Scotcher M, Chang SY, Zhang SL. Maternal diabetes programs hypertension and kidney injury in offspring. *Pediatr Nephrol* 2010;25:1319–29.
11. Tran S, Chen YW, Chenier I, *et al*. Maternal diabetes modulates renal morphogenesis in offspring. *J Am Soc Nephrol* 2008;19:943–52.
12. Zhang SL, Chen YW, Tran S, Chenier I, Hébert MJ, Ingelfinger JR. Reactive oxygen species in the presence of high glucose alter ureteric bud morphogenesis. *J Am Soc Nephrol* 2007;18:2105–15.
13. Chen YW, Chenier I, Chang SY, Tran S, Ingelfinger JR, Zhang SL. High glucose promotes nascent nephron apoptosis via NF- κ B and p53 pathways. *Am J Physiol Renal Physiol* 2011;300:F147–56.
14. Declèves AE, Mathew AV, Cunard R, Sharma K. AMPK mediates the initiation of kidney disease induced by a high-fat diet. *J Am Soc Nephrol* 2011;22:1846–55.
15. Odermatt A. The Western-style diet: a major risk factor for impaired kidney function and chronic kidney disease. *Am J Physiol Renal Physiol* 2011;301:F919–31.
16. Soumura M, Kume S, Isshiki K, *et al*. Oleate and eicosapentaenoic acid attenuate palmitate-induced inflammation and apoptosis in renal proximal tubular cell. *Biochem Biophys Res Commun* 2010;402:265–71.
17. Foster MC, Hwang SJ, Porter SA, Massaro JM, Hoffmann U, Fox CS. Fatty kidney, hypertension, and chronic kidney disease: the Framingham Heart Study. *Hypertension* 2011;58:784–90.
18. Chandra A, Neeland JJ, Berry JD, *et al*. The relationship of body mass and fat distribution with incident hypertension: observations from the Dallas Heart Study. *J Am Coll Cardiol* 2014;64:997–1002.
19. Hajri T, Han XX, Bonen A, Abumrad NA. Defective fatty acid uptake modulates insulin responsiveness and metabolic responses to diet in CD36-null mice. *J Clin Invest* 2002;109:1381–9.
20. Kang HM, Ahn SH, Choi P, *et al*. Defective fatty acid oxidation in renal tubular epithelial cells has a key role in kidney fibrosis development. *Nat Med* 2015;21:37–46.
21. Kennedy DJ, Kuchibhotla S, Westfall KM, Silverstein RL, Morton RE, Febbraio M. A CD36-dependent pathway enhances macrophage and adipose tissue inflammation and impairs insulin signalling. *Cardiovasc Res* 2011;89:604–13.
22. Kennedy DJ, Chen Y, Huang W, *et al*. CD36 and Na/K-ATPase- α 1 form a proinflammatory signaling loop in kidney. *Hypertension* 2013;61:216–24.
23. Ishimura S, Furuhashi M, Watanabe Y, *et al*. Circulating levels of fatty acid-binding protein family and metabolic phenotype in the general population. *PLoS One* 2013;8:e81318.
24. Furuhashi M, Ishimura S, Ota H, *et al*. Serum fatty acid-binding protein 4 is a predictor of cardiovascular events in end-stage renal disease. *PLoS One* 2011;6:e27356.
25. Yeung DC, Xu A, Tso AW, *et al*. Circulating levels of adipocyte and epidermal fatty acid-binding proteins in relation to nephropathy staging and macrovascular complications in type 2 diabetic patients. *Diabetes Care* 2009;32:132–4.
26. Tanaka M, Furuhashi M, Okazaki Y, *et al*. Ectopic expression of fatty acid-binding protein 4 in the glomerulus is associated with proteinuria and renal dysfunction. *Nephron Clin Pract* 2014;128:345–51.
27. Okazaki Y, Furuhashi M, Tanaka M, *et al*. Urinary excretion of fatty acid-binding protein 4 is associated with albuminuria and renal dysfunction. *PLoS One* 2014;9:e115429.

28. Prior LJ, Velkoska E, Watts R, Cameron-Smith D, Morris MJ. Undernutrition during suckling in rats elevates plasma adiponectin and its receptor in skeletal muscle regardless of diet composition: a protective effect? *Int J Obes (Lond)* 2008;32:1585–94.
29. Velkoska E, Cole TJ, Dean RG, Burrell LM, Morris MJ. Early undernutrition leads to long-lasting reductions in body weight and adiposity whereas increased intake increases cardiac fibrosis in male rats. *J Nutr* 2008;138:1622–7.
30. Bruce CR, Hoy AJ, Turner N, et al. Overexpression of carnitine palmitoyltransferase-1 in skeletal muscle is sufficient to enhance fatty acid oxidation and improve high-fat diet-induced insulin resistance. *Diabetes* 2009;58:550–8.
31. Murrow BA, Hoehn KL. Mitochondrial regulation of insulin action. *Int J Biochem Cell Biol* 2010;42:1936–9.
32. Kennedy AJ, Ellacott KL, King VL, Hasty AH. Mouse models of the metabolic syndrome. *Dis Model Mech* 2010;3:156–66.
33. Kim HJ, Vaziri ND, Norris K, An WS, Quiroz Y, Rodriguez-Iturbe B. High-calorie diet with moderate protein restriction prevents cachexia and ameliorates oxidative stress, inflammation and proteinuria in experimental chronic kidney disease. *Clin Exp Nephrol* 2010;14:536–47.
34. Hamdani N, Franssen C, Lourenço A, et al. Myocardial titin hypophosphorylation importantly contributes to heart failure with preserved ejection fraction in a rat metabolic risk model. *Circ Heart Fail* 2013;6:1239–49.
35. Baines RJ, Chana RS, Hall M, Febbraio M, Kennedy D, Brunskill NJ. CD36 mediates proximal tubular binding and uptake of albumin and is upregulated in proteinuric nephropathies. *Am J Physiol Renal Physiol* 2012;303:F1006–14.
36. Susztak K, Ciccone E, McCue P, Sharma K, Böttinger EP. Multiple metabolic hits converge on CD36 as novel mediator of tubular epithelial apoptosis in diabetic nephropathy. *PLoS Med* 2005;2:e45.
37. Okamura DM, López-Guisa JM, Koelsch K, Collins S, Eddy AA. Atherogenic scavenger receptor modulation in the tubulointerstitium in response to chronic renal injury. *Am J Physiol Renal Physiol* 2007;293:F575–85.
38. Xu A, Vanhoutte PM. Adiponectin and adipocyte fatty acid binding protein in the pathogenesis of cardiovascular disease. *Am J Physiol Heart Circ Physiol* 2012;302:H1231–40.
39. el Nahas AM, Bassett AH, Cope GH, Le Carpentier JE. Role of growth hormone in the development of experimental renal scarring. *Kidney Int* 1991;40:29–34.
40. Véniant M, Heudes D, Clozel JP, Bruneval P, Ménard J. Calcium blockade versus ACE inhibition in clipped and unclipped kidneys of 2K-1C rats. *Kidney Int* 1994;46:421–9.
41. Roduit R, Masiello P, Wang SP, Li H, Mitchell GA, Prentki M. A role for hormone-sensitive lipase in glucose-stimulated insulin secretion: a study in hormone-sensitive lipase-deficient mice. *Diabetes* 2001;50:1970–5.